NANO LETTERS

Letter

Cite This: Nano Lett. 2017, 17, 7075-7079

pubs.acs.org/NanoLett

Real-Space Observation of Nonvolatile Zero-Field Biskyrmion Lattice Generation in MnNiGa Magnet

Licong Peng,[†,‡] Ying Zhang,*[,†] Wenhong Wang,[†] Min He,[†,‡] Lailai Li,[†,‡] Bei Ding,[†,‡] Jianqi Li,[†,‡] Young Sun,*[,†,‡] X.-G. Zhang,[§] Jianwang Cai,[†,‡] Shouguo Wang,[∥] Guangheng Wu,[†] and Baogen Shen[†,‡]

[†]Beijing National Laboratory for Condensed Matter Physics, Institute of Physics, Chinese Academy of Sciences, Beijing 100190, China

[‡]School of Physical Sciences, University of Chinese Academy of Sciences, Beijing 100049, China

[§]Department of Physics and the Quantum Theory Project, University of Florida, Gainesville, Florida 32611, United States

[∥]School of Materials Science and Engineering, University of Science and Technology Beijing, Beijing 100083, China

Supporting Information

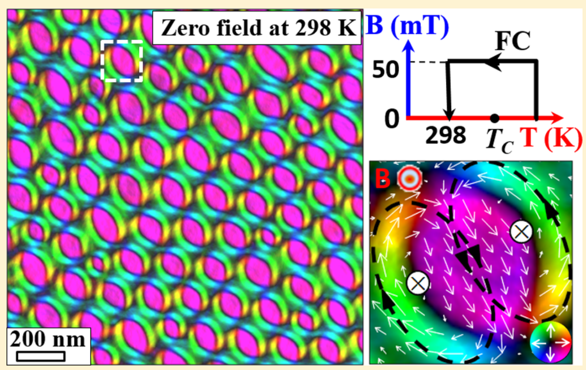

ABSTRACT: Magnetic skyrmions, particular those without the support of external magnetic fields over a wide temperature region, are promising as alternative spintronic units to overcome the fundamental size limitation of conventional magnetic bits. In this study, we use in situ Lorentz microscope to directly demonstrate the generation and sustainability of robust biskyrmion lattice at zero magnetic field over a wide temperature range of 16−338 K in MnNiGa alloy. This procedure includes a simple field-cooling manipulation from 360 K (higher than Curie temperature $T_C \sim 350$ K), where topological transition easily occurs by adapting the short-range magnetic clusters under a certain magnetic field. The biskyrmion phase is favored upon cooling below T_C. Once they are generated, the robust high-density biskyrmions persist even after removing the external magnetic field due to the topological protection and the increased energy barrier.

KEYWORDS: *Biskyrmion lattice, zero field, field-cooling manipulation, topological transition, Lorentz TEM, MnNiGa*

Magnetic skyrmions have drawn particular attention because the topologically stable nanometric spin textures[1,2] together with a variety of manipulation options[3−5] exhibit the potential to overcome the density limitation in conventional magnetic storage media, thereby prompting the production of next-generation spintronic devices. The skyrmion state, which is characteristic of a nonlinear continuum model, can be experimentally induced under nonequilibrium conditions or stabilized via external fields or the proliferation of topological defects.[6] A perpendicular magnetic field is typically required to transform the helical stripes into skyrmions within a narrow temperature range near Curie temperature (T_C) and below room temperature in prominent symmetry-broken chiral materials such as MnSi,[7,8] $(Fe_{1-x}Co_x)Si$,[9] and FeGe.[3,10] Furthermore, the topological nanometer domains in several classes of materials including ferromagnetic multilayers with asymmetric interface,[11,12] artificially patterned films,[13,14] and uniaxial dipolar bulk magnets,[5,15,16] have been explored. For application in information storage, the existence of skyrmion lattice without the requirement of external fields over a wide temperature range is critically appealing.

Recently, developments in extending metastable skyrmions toward a lower temperature range have been reported via thermal manipulation in bulk chiral magnets, such as $Co_8Zn_8Mn_4$ with a field-cooling (FC) procedure[17] and MnSi with current-pulse quenching.[18] Rapid cooling from the equilibrium skyrmion state below T_C is asserted to be critical to form extended metastable skyrmions for both the aforementioned manipulations evidenced by neutron diffraction[17] and Hall resistivity measurement,[18] respectively. The metastable skyrmions at zero magnetic field are extended below 280 K after FC manipulation in $Co_8Zn_8Mn_4$; however, the magnetic field required to form skyrmions remains unchanged within the original skyrmion region of 284−300 K.[17] The temperature region has been extended without realizing zero-field skyrmions in chiral MnSi (below 30 K)[18] and with an elongated structure at zero field in $Fe_{0.5}Co_{0.5}Si$ (below 50 K).[19] In certain centrosymmetric materials such as $La_{1-x}Sr_xMnO_3$ (x = 0.175),[20] $La_{2-2x}Sr_{1+2x}Mn_2O_7$ (x = 0.315),[15] and $BaFe_{12-x-0.05}Sc_xMg_{0.05}O_{19}$ (x = 1.8),[5] magnetic bubbles with different spin configurations can be easily identified via high spatial resolution Lorentz microscopy. However, such bubbles are difficult to be distinguished using indirect measurements if their spin configurations are topologically equivalent to

Received: September 5, 2017
Revised: September 20, 2017
Published: October 9, 2017

skyrmions. For example, magnetic bubbles and biskyrmions obtained via FC and ZFC, respectively, from the same $La_{2-2x}Sr_{1+2x}Mn_2O_7$ (x = 0.315)[15] were clearly distinguished by Lorentz microscopy. Therefore, in situ Lorentz transmission electron microscopy (L-TEM) can be used as a direct method to demonstrate the generation and extension behavior of zero-field magnetic skyrmions, which interprets the evolution of microscopic spin configuration for exploring new mechanism.

In the present work, the generation of zero-field biskyrmion lattice after thermal manipulation is directly demonstrated via L-TEM in MnNiGa, thereby completely substituting the randomly distributed biskyrmions in the temperature range of 16−338 K.[16] We find that an appropriate FC procedure that starts from a temperature above T_C favors the setting of topological transition to generate robust biskyrmions, which is different from the previous manipulation in chiral material.[17] Moreover, the microscopic short-range magnetic correlations above T_C, as evidenced by electron spin resonance (ESR) spectra of up to 400 K, play a critical role in generating and stabilizing biskyrmions below T_C in MnNiGa alloy. Once the biskyrmion phase has been generated, the topological protection and the increased energy barrier help to sustain the nonvolatile biskyrmion lattice at zero field over a wide temperature range of 16−338 K below T_C.

The as-cast polycrystalline $(Mn_{1-x}Ni_x)_{65}Ga_{35}$ (x = 0.5), called MnNiGa, is the same as that used in our previous work,[16,21] where the basic information and the topological properties have been demonstrated. The observed edge area ranges from 40 to 100 nm with slight thickness gradient while moving away from the edge. The crystallographic orientation of the observed edge area is near [001] direction. The biskyrmion evolution behavior with thermal manipulation is observed using Lorentz TEM (JEOL2100F) equipped with a liquid-nitrogen or a liquid-helium holder. Quantitative in-plane magnetization is analyzed using the transport-of-intensity equation (TIE)[22] with the software package QPt. The magnetic field applied perpendicularly to the thin plate is induced by the magnetic objective lens of the microscope. The specimen for L-TEM observation is prepared via traditional polishing, dimpling, and subsequently, ion milling. ESR study is performed using a JEOL FA-200 ESR spectrometer at 9.4 GHz.

Figure 1a schematically depicts the detailed FC process with the corresponding L-TEM images acquired at marked conditions. The existence of high-density biskyrmion lattice at zero field is confirmed at 298 K in Figure 1b and at 16 K in Figure 1c after the optimized FC manipulation (B = 50 mT) has been conducted. The elimination of the magnetic field only makes the biskyrmions slightly larger but does not change their topological configuration and density, which are determined by the experimental conditions to generate biskyrmions (Figure 2). Biskyrmion density is remarkably enhanced via FC manipulation compared with the randomly distributed biskyrmions induced purely by the magnetic field at the same temperature, as shown in Figure 1. Notably, these zero-field biskyrmions remain extremely robust across time in a field-free environment even after three months at room temperature, thereby exhibiting potential applications in nonvolatile memory devices.

To clearly identify the spin configuration of the biskyrmions after FC manipulation, the in-plane magnetic component distribution based on TIE for a selected biskyrmion is shown in Figure 1d. The spin texture of the biskyrmion is composed of two skyrmions with opposite helicities (i.e, clockwise and

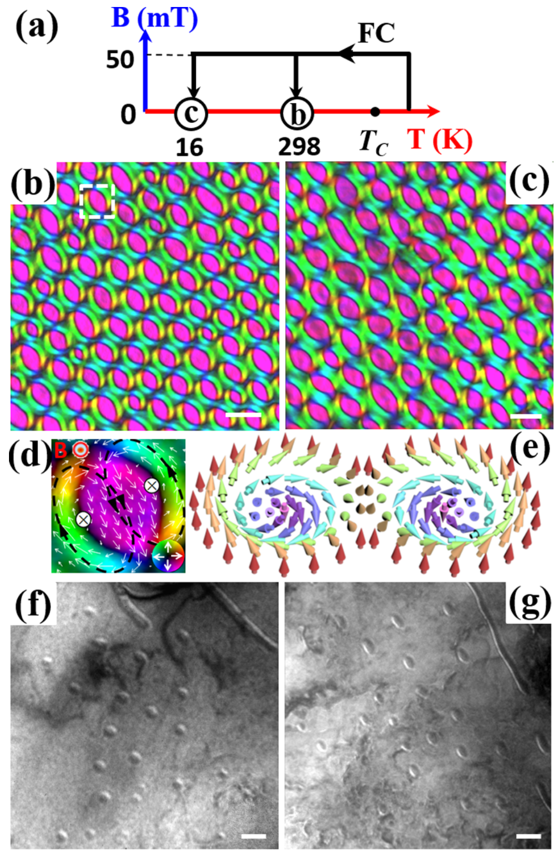

Figure 1. Comparison between the nonvolatile field-free biskyrmion lattice after FC manipulation and the randomly distributed biskyrmions induced purely by the magnetic field in MnNiGa. (a) Schematic illustration of the FC procedure. L-TEM images of high-density biskyrmion lattice at zero magnetic field at (b) 298 K and (c) 16 K after FC manipulation. (d) In-plane magnetization of the selected biskyrmion configuration from (b). (e) Schematic biskyrmion spin configuration. L-TEM images of the magnetic field-induced scattered biskyrmions at (f) 298 K (250 mT) and (g) 16 K (480 mT) without the FC procedure. The scale bars are 200 nm.

counterclockwise spin curl orientation) but the same central spin direction at the core sites, as schematically shown in Figure 1e. This configuration distinguishes with the traditional bubbles[15] and is the same as the biskyrmions reported in previous studies[15,16,23] and has been proven to be energetically stable in centrosymmetric magnets.[24]

The detailed biskyrmion evolution dependent on temperature and magnetic field is depicted in Figure 2 with the experimental procedures schematically illustrated at the top. When a low magnetic field of 50 mT is applied at room temperature (298 K), the spontaneous ground state of the stripe domains remains unchanged, as shown in Figure 2a. As it gradually approaches T_C, the stripe domain appears to be pinched off with more biskyrmions at higher temperatures. The distorted hexagonal biskyrmion lattice at 335 K is shown with slightly different contrast in Figure 2b due to the thickness gradient[15,25] and thermal fluctuation. The magnetic domains lose contrast at ∼345 K (Figure 2c) due to the decreased domain size and increased thermal fluctuation. When the temperature is increased to 360 K (above T_C = ∼350 K) and then decreased to room temperature while applying a magnetic field of 50 mT during the cooling process, high-density magnetic biskyrmions with a homogeneous distribution are

DOI: 10.1021/acs.nanolett.7b03792
Nano Lett. 2017, 17, 7075−7079

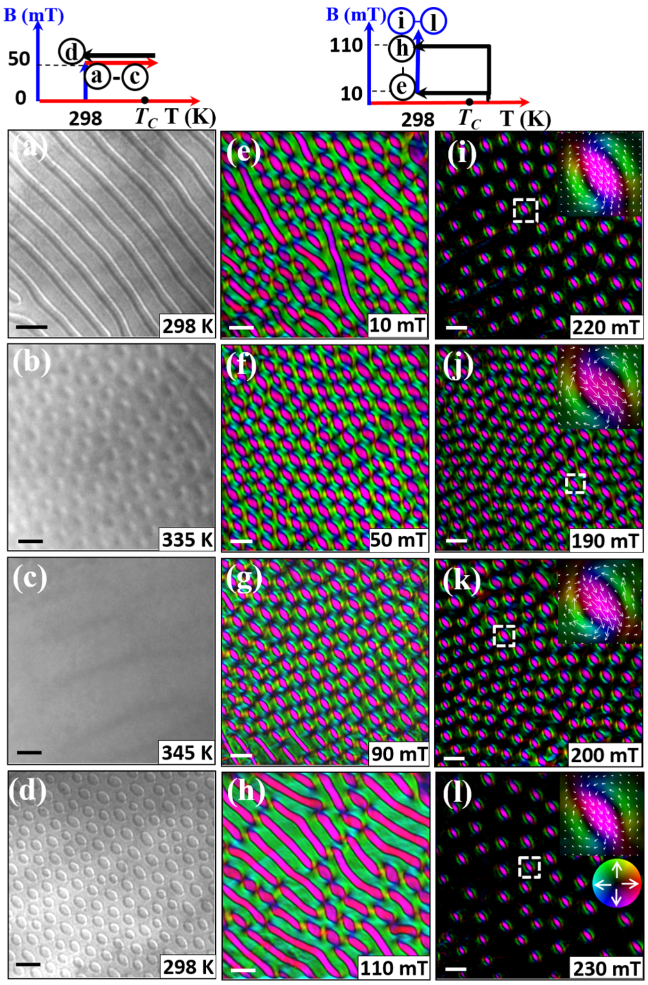

Figure 2. L-TEM images demonstrating the biskyrmion generation and sustainability via appropriate FC manipulation in MnNiGa. L-TEM images acquired under a magnetic field of 50 mT at (a) 298 K, (b) 335 K, (c) 345 K, and (d) back to 298 K. (e−h) L-TEM images of the magnetic domain distribution at 298 K after FC manipulation from 360 K under different magnetic fields. (i−l) Biskyrmion distribution after increasing the magnetic fields to complete skyrmion state based on the corresponding residual magnetic domains shown in (e−h). Insets in panels i−l: in-plane magnetization of the selected single biskyrmion. The experimental procedures are shown on top of the column. The scale bars are 200 nm.

formed as shown in Figure 2d. The removal of the magnetic field at this state causes only a slight increase in size. To elucidate the origin of the biskyrmion state, we have set different fixed magnetic fields (10, 50, 90, and 110 mT) for each FC procedure and discovered that the magnetic field significantly influences the biskyrmion density at room temperature, as shown in Figure 2e−2h. At an optimized magnetic field of approximately 50 mT, the biskyrmion phase is dominant (Figure 2f), compared with the mixed stripe and biskyrmion phase at lower (Figure 2e) and higher (Figures 2g,h) magnetic fields. If the sample is cooled at zero magnetic field (ZFC), then the regular stripe domain directly pops up without biskyrmions. However, when the magnetic field is too strong, the nucleation sites will be forced to agglomerate, thereby reducing biskyrmion density (Figure 2h). Thus, the magnetic field plays a critical role during the FC process, and an optimized magnetic field exists to generate the biskyrmion phase with the highest density. When the magnetic fields are further increased to 220, 190, 200, and 230 mT, as shown respectively in Figure 2i−l, the mixed stripes and biskyrmions evolve into complete biskyrmion state with different densities. Notably, the newly generated biskyrmions from the residual stripes exhibit low density after further increasing the magnetic field. This phenomenon consists with the low-density equilibrium biskyrmion phase that is directly induced by magnetic fields as shown in Figure 1f. Furthermore, the biskyrmion lattice derived from FC manipulation persists even after the removal of magnetic fields across the temperature range of 16−338 K in MnNiGa.

The overall phase diagrams for the evolution of biskyrmions as a function of magnetic field and temperature without and with the FC procedure are summarized in Figure 3a,b,

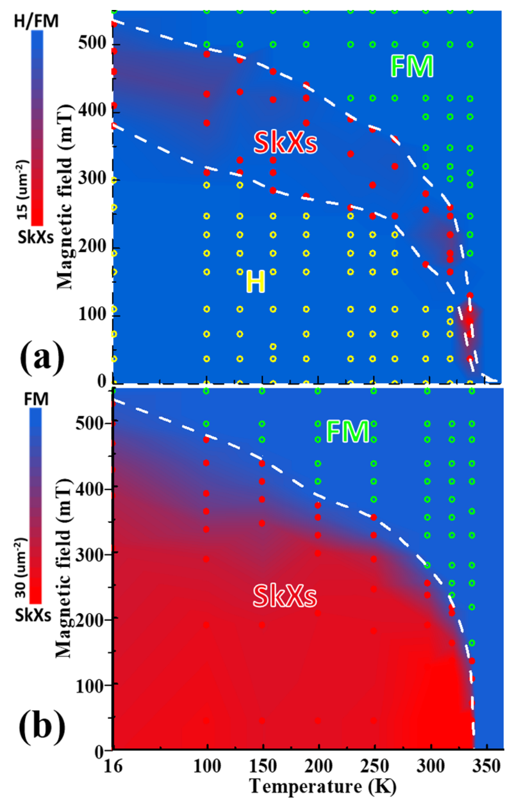

Figure 3. Overall phase diagrams obtained by contour mapping biskyrmion density as a function of external magnetic field (B) and temperature (T) based on in situ L-TEM observation of skyrmion evolution from (a) ground stripe domains at different temperatures and (b) residual domains after the optimized 50 mT FC manipulation. The colorful dots denote the experimental points, whereas the dashed lines serve as guides for the biskyrmion phase region. The color scale indicates biskyrmion density per square micrometer. SkXs stands for biskyrmion phase, FM for ferromagnetic phase, and H for helical stripes.

respectively, via contour mapping biskyrmion density based on L-TEM images. As shown in Figure 3a, the threshold and annihilation magnetic fields for thermodynamically stable biskyrmions are outlined as white dashed lines over the wide temperature range of 16−338 K. The magnetic field required to generate biskyrmions decreases with increasing temperature and is substantially reduced near T_C, which corresponds to a significantly decreased anisotropy (H_a). The red-colored area near T_C in Figure 3a only illustrates that the biskyrmion density is remarkably higher than those far from T_C but the equilibrium

DOI: 10.1021/acs.nanolett.7b03792
Nano Lett. 2017, 17, 7075−7079

biskyrmions exist across the entire temperature range of 16–338 K. The equilibrium biskyrmion phase diagram of MnNiGa (Figure 3a) intrinsically differs from that of chiral magnets, where the skyrmion phase exists only within the narrow temperature range below T_C.[17,18] Consequently, FC manipulation in chiral magnets only extends the metastable skyrmions below the equilibrium temperature range and is easily influenced by the cooling rate.[17,18] After an optimized 50 mT FC manipulation from 360 K to below T_C in MnNiGa, dominant biskyrmions are obtained at different temperatures at zero field, and the biskyrmion density and evolution is summarized in Figure 3b. The high-density red-colored area with nonvolatile zero-field biskyrmions covers the entire temperature range after FC manipulation (Figure 3b).

Topological transition occurs while undergoing magnetic phase transitions or by overcoming the energy barrier between the skyrmion and ferromagnetic phases.[18,26] Lacking direct measurements of the energy barrier, understanding of skyrmion transition relies on indirect means such as Monte Carlo simulation of the free-energy landscape between skyrmion and ferromagnetic states.[27] Our measurement of the skyrmion density as a function of magnetic field and temperature allows the energy barrier to be extracted using a phenomenological free-energy model. The temperature dependence of the extracted energy barrier is plotted in Figure S2 based on the derivate model and the experimental results (see the details in the Supporting Information). The energy barrier is reduced as temperature increases and near T_C the barrier drops by 2 orders of magnitude. Thus, an energetically favorable biskyrmion embryos generated through appropriate FC manipulation can be preserved below T_C. Notably, the high-density biskyrmions generated through this FC process have considerably wider T–B window (red area in Figure 3b), and the obtained biskyrmions are free from magnetic fields and remarkably robust because of energetically increased potential barrier during cooling[18] and the topological protection effects. Compared with chiral magnets,[17] in which the FC procedure starts from the skyrmion equilibrium state below T_C, our phase diagram in Figure 3b is obtained with the FC procedure starting above T_C.

ESR spectra are measured at different temperatures, as shown in Figure 4, to verify the nature of the microscopic magnetic structure above T_C. In addition to the paramagnetic resonance line, the low-field resonance line is a characteristic of short-range magnetic clusters, where local magnetic correlations generate an effective inner magnetic field, and consequently, induce resonance at a lower field. As the temperature increases, the low-field resonance line shifts smoothly toward a higher field and the magnetic clusters gradually become smaller until they become completely disordered above ~400 K. The microscopic magnetic clusters contribute to the biskyrmion formation in MnNiGa, similar to the previous findings in which the clusters serve as precursors in favor of the phase formation.[10,28−30] The applied magnetic fields help to align, order, and grow magnetic clusters. When the size of magnetic clusters reaches an optimized value, the embryo of the topological biskyrmion phase is energetically favored by the competition between external magnetic field-induced anisotropy and short-range magnetic interactions. The cooling of these microscopic clusters with the aid of a low magnetic field leads to the development of biskyrmions below T_C (Figure 2e–h). The magnetic biskyrmions generated during the FC manipulation remain robust even after removing the magnetic field because the topological protection and the increased energy barrier help to prevent spontaneous transition to the stripe domains.

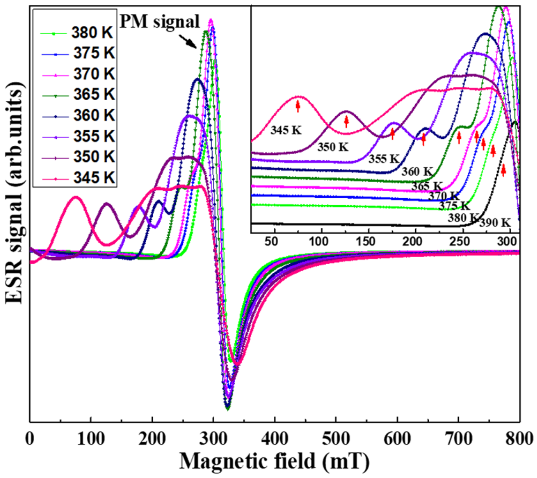

Figure 4. Experimental evidence of short-range magnetic clusters above T_C based on ESR spectra. The temperature dependence of ESR spectra indicate the existence and continuous evolution of short-range magnetic clusters above T_C, which is presented with the emergence of the low-field resonance lines that are marked by arrows, in addition to the paramagnetic resonance signal.

In conclusion, the generation and sustainability of the robust field-free biskyrmion lattice via appropriate magnetic FC manipulation from above T_C have been directly demonstrated in MnNiGa thin flake over a wide temperature range of 16–338 K. The microscopic origin of this nonvolatile metastable biskyrmion phase has been discussed based on the temperature dependence of energy landscape and the evolution of the microscopic magnetic structure above and near T_C in MnNiGa alloy. The generation of high-density field-free biskyrmion lattice at room temperature via a simple FC procedure exhibits potential applications in nonvolatile memory devices and provides a direct reference for exploring novel mechanisms.

■ ASSOCIATED CONTENT

Supporting Information

The Supporting Information is available free of charge on the ACS Publications website at DOI: 10.1021/acs.nanolett.7b03792.

Calculation of the temperature-dependent energy barrier between skyrmion and ferromagnetic phase (PDF)

■ AUTHOR INFORMATION

Corresponding Authors

*E-mail: zhangy@iphy.ac.cn.

*E-mail: youngsun@iphy.ac.cn.

ORCID

Ying Zhang: 0000-0001-5476-1524

Young Sun: 0000-0001-8879-3508

Notes

The authors declare no competing financial interest.

■ ACKNOWLEDGMENTS

We thank Dr. Zhao, T. Y.; Dai, X.; Sun, J. R.; Chai, Y. S.; Yang, Y. F.; Meng, Z. Y., and Cabra D. for helpful discussions. This work was supported by the National Basic Research Program of

DOI: 10.1021/acs.nanolett.7b03792
Nano Lett. 2017, 17, 7075–7079

China (2015CB921401), The National Key Research and Development Program of China (No. 2016YFA0300300), National Natural Science Foundation of China (Grants 11374349, 51590880, 51431009, 51371192, 51561145003, 51471183), Youth Innovation Promotion Association, CAS, 2015004.

■ REFERENCES

(1) Nagaosa, N.; Tokura, Y. *Nat. Nanotechnol.* **2013**, *8* (12), 899–911.
(2) Yu, X. Z.; Onose, Y.; Kanazawa, N.; Park, J. H.; Han, J. H.; Matsui, Y.; Nagaosa, N.; Tokura, Y. *Nature* **2010**, *465* (17), 901–904.
(3) Zhao, X.; Jin, C.; Wang, C.; Du, H.; Zang, J.; Tian, M.; Che, R.; Zhang, Y. *Proc. Natl. Acad. Sci. U. S. A.* **2016**, *113* (18), 4918–4923.
(4) Yu, X. Z.; Kanazawa, N.; Zhang, W. Z.; Nagai, T.; Hara, T.; Kimoto, K.; Matsui, Y.; Onose, Y.; Tokura, Y. *Nat. Commun.* **2012**, *3*, 988.
(5) Yu, X. Z.; Shibata, K.; Koshibae, W.; Tokunaga, Y.; Kaneko, Y.; Nagai, T.; Kimoto, K.; Taguchi, Y.; Nagaosa, N.; Tokura, Y. *Phys. Rev. B: Condens. Matter Mater. Phys.* **2016**, *93* (13), 134417.
(6) Rößler, U. K.; Bogdanov, A. N.; Pfleiderer, C. *Nature* **2006**, *442* (17), 797–801.
(7) Mühlbauer, S.; Binz, B.; Jonietz, F.; Pfleiderer, C.; Rosch, A.; Neubauer, A.; Georgii, R.; Böni, P. *Science* **2009**, *323* (6048), 915–919.
(8) Neubauer, A.; Pfleiderer, C.; Binz, B.; Rosch, A.; Ritz, R.; Niklowitz, P. G.; Boni, P. *Phys. Rev. Lett.* **2009**, *102* (18), 186602.
(9) Grigoriev, S. V.; Chernyshov, D.; Dyadkin, V. A.; Dmitriev, V.; Maleyev, S. V.; Moskvin, E. V.; Menzel, D.; Schoenes, J.; Eckerlebe, H. *Phys. Rev. Lett.* **2009**, *102* (3), 037204.
(10) Wilhelm, H.; Baenitz, M.; Schmidt, M.; Rößler, U. K.; Leonov, A. A.; Bogdanov, A. N. *Phys. Rev. Lett.* **2011**, *107* (12), 127203.
(11) Pollard, S. D.; Garlow, J. A.; Yu, J.; Wang, Z.; Zhu, Y.; Yang, H. *Nat. Commun.* **2017**, *8*, 14761.
(12) Jiang, W.; Upadhyaya, P.; Zhang, W.; Yu, G.; Jungfleisch, M. B.; Fradin, F. Y.; Pearson, J. E.; Tserkovnyak, Y.; Wang, K. L.; Heinonen, O.; te Velthuis, S. G. E.; Hoffmann, A. *Science* **2015**, *349* (6245), 283–286.
(13) Miao, B. F.; Sun, L.; Wu, Y. W.; Tao, X. D.; Xiong, X.; Wen, Y.; Cao, R. X.; Wang, P.; Wu, D.; Zhan, Q. F.; You, B.; Du, J.; Li, R. W.; Ding, H. F. *Phys. Rev. B: Condens. Matter Mater. Phys.* **2014**, *90*, 174411.
(14) Sun, L.; Cao, R. X.; Miao, B. F.; Feng, Z.; You, B.; Wu, D.; Zhang, W.; Hu, A.; Ding, H. F. *Phys. Rev. Lett.* **2013**, *110* (16), 167201.
(15) Yu, X. Z.; Tokunaga, Y.; Kaneko, Y.; Zhang, W. Z.; Kimoto, K.; Matsui, Y.; Taguchi, Y.; Tokura, Y. *Nat. Commun.* **2014**, *5*, 3198.
(16) Wang, W.; Zhang, Y.; Xu, G.; Peng, L.; Ding, B.; Wang, Y.; Hou, Z.; Zhang, X.; Li, X.; Liu, E.; Wang, S.; Cai, J.; Wang, F.; Li, J.; Hu, F.; Wu, G.; Shen, B.; Zhang, X. X. *Adv. Mater.* **2016**, *28* (32), 6887–6893.
(17) Karube, K.; White, J. S.; Reynolds, N.; Gavilano, J. L.; Oike, H.; Kikkawa, A.; Kagawa, F.; Tokunaga, Y.; Rønnow, H. M.; Tokura, Y.; Taguchi, Y. *Nat. Mater.* **2016**, *15* (12), 1237–1242.
(18) Oike, H.; Kikkawa, A.; Kanazawa, N.; Taguchi, Y.; Kawasaki, M.; Tokura, Y.; Kagawa, F. *Nat. Phys.* **2015**, *12* (1), 62–66.
(19) Milde, P.; Köhler, D.; Seidel, J.; Eng, L. M.; Bauer, A.; Chacon, A.; Kindervater, J.; Mühlbauer, S.; Pfleiderer, C.; Buhrandt, S.; Schütte, C.; Rosch, A. *Science* **2013**, *340* (5), 1076–1080.
(20) Yu, X.; Tokunaga, Y.; Taguchi, Y.; Tokura, Y. *Adv. Mater.* **2017**, *29* (3), 1603958.
(21) Peng, L.; Zhang, Y.; He, M.; Ding, B.; Wang, W.; Li, J.; Wang, S.; Cai, J.; Wu, G.; Liu, J. P.; Kramer, M. J.; Shen, B. *npj Quant. Mater.* **2017**, DOI: 10.1038/s41535-017-0034-7.
(22) Ishizuka, K.; Allman, B. *J. Electron Microsc.* **2005**, *54* (3), 191–197.
(23) Lee, J. C. T.; Chess, J. J.; Montoya, S. A.; Shi, X.; Tamura, N.; Mishra, S. K.; Fischer, P.; McMorran, B. J.; Sinha, S. K.; Fullerton, E. E.; Kevan, S. D.; Roy, S. *Appl. Phys. Lett.* **2016**, *109* (2), 022402.
(24) Lilliehöök, D.; Lejnell, K.; Karlhede, A.; Sondhi, S. L. *Phys. Rev. B: Condens. Matter Mater. Phys.* **1997**, *56* (11), 6805–6809.
(25) Park, H. S.; Yu, X.; Aizawa, S.; Tanigaki, T.; Akashi, T.; Takahashi, Y.; Matsuda, T.; Kanazawa, N.; Onose, Y.; Shindo, D.; Tonomura, A.; Tokura, Y. *Nat. Nanotechnol.* **2014**, *9* (5), 337–342.
(26) Romming, N.; Hanneken, C.; Menzel, M.; Bickel, J. E.; Wolter, B.; von Bergmann, K.; Kubetzka, A.; Wiesendanger, R. *Science* **2013**, *341* (6146), 636–639.
(27) Hagemeister, J.; Romming, N.; von Bergmann, K.; Vedmedenko, E. Y.; Wiesendanger, R. *Nat. Commun.* **2015**, *6*, 8455.
(28) Wilhelm, H.; Baenitz, M.; Schmidt, M.; Naylor, C.; Lortz, R.; Rößler, U. K.; Leonov, A. A.; Bogdanov, A. N. *J. Phys.: Condens. Matter* **2012**, *24* (29), 294204.
(29) Wilson, M. N.; Butenko, A. B.; Bogdanov, A. N.; Monchesky, T. L. *Phys. Rev. B: Condens. Matter Mater. Phys.* **2014**, *89* (9), 094411.
(30) Nagao, M.; So, Y.-G.; Yoshida, H.; Isobe, M.; Hara, T.; Ishizuka, K.; Kimoto, K. *Nat. Nanotechnol.* **2013**, *8* (5), 325–328.

DOI: 10.1021/acs.nanolett.7b03792
Nano Lett. 2017, 17, 7075–7079